

# Two Methods of Amplification of Coherent Extreme Ultraviolet Radiation During Harmonic Generation in Plasmas<sup>1</sup>

R. A. Ganeev

*The Guo China-US Photonics Laboratory, Changchun Institute of Optics, Fine Mechanics and Physics,  
Changchun, 130033 China*

*e-mail: rashid\_ganeev@mail.ru*

Received December 30, 2017

**Abstract**—Different recently revealed approaches of harmonic enhancement in plasmas are reviewed. The 4-step analytical model of resonant enhancement of high-order harmonic generation is extended to the systems possessing resonant transitions of inner-shell electrons. Role of inelastic scattering is discussed by simulation of excited state's population dynamics. The enhancement of harmonics in the In plasma using different pumps is analyzed to prove the concept. We also discuss the plasma emission and harmonic generation spectra in the case of resonance enhancement of single harmonic using various laser-produced plasmas. The analysis of these spectra showed that the enhancement of harmonics depended on the oscillator strengths of the nearby ionic transitions rather than the plasma emission transitions. Finally, we review some recent experimental studies of the phase-matching of high-order harmonic generation in multi-jet plasmas.

DOI: 10.1134/S0030400X18060073

## 1. MODEL OF RESONANT HIGH-ORDER HARMONIC GENERATION IN MULTI-ELECTRON SYSTEMS

### 1.1. Introduction

High-order harmonic generation (HHG) in the plasma media produced on the surface of solid targets by laser ablation has been an important part of studies in laser physics during last 20 years due to potential applications of short-wavelength coherent radiation in laser holography, lithography, medicine, and attophysics [1]. The only limiting factor of the strong-field HHG is its low conversion efficiency to harmonics. There are several ways to increase conversion efficiency (resonance-induced growth of harmonic yield, application of nanoparticles and clusters as the non-linear media, use of quasi-phase-matching concept, etc.). Among them, resonance-induced growth of single harmonic is one of the simplest and most successful methods [2, 3]. Since first observation of this phenomenon of resonant HHG in the indium plasma [2], some other plasma media [3, 4] were identified for the potential enhancement of the single harmonics due to their spectral closeness with the ionic transitions possessing strong oscillator strengths.

Analogous attempts for noble gases were reported as well, which, however, failed to experimentally demonstrate the resonant HHG, even in cases when such an enhancement was expected [5–8]. This fact

can be attributed to the availability of a much wider range of target materials for plasma HHG compared to a few commonly used gases, which significantly increases the possibility of the resonance of an ionic transition in plasma media with a harmonic wavelength. However, despite the broad range of spectral properties of various laser plasmas, resonant HHG was reported only for a few strong spectral lines in the In, Cr, Mn, Sb, and As plasmas. The resonant enhancement factor was varied between 2 and 80 for different laser plasmas. The only difference between the HHG experiments with noble gases and laser plasmas is the fact that latter media are usually singly charged at the moment of interaction with strong probe pulse, while the noble gases are not. This difference motivates to seek for a model, which ultimately benefits from sufficient degree of ionization of the media.

Although some possibilities of non-resonant HHG in the intra-atomic dynamics of electron have been theoretically predicted [9], the experiments [2–4] have shown that return of the electron to the parent particle predicted by the 3-step model [10] is crucial for existence of resonant HHG. As a result the theories, which do not include continuum states [5, 11], cannot explain resonant HHG.

Many models describe enhancement of HHG yield in the presence of strong intra-atomic resonance as a consequence of enhanced probability of bound-bound transition [6, 12–15] or multiphoton ionization [16] at the conditions of multiphoton resonance. Multipho-

<sup>1</sup> The article is published in the original.

ton resonant transitions cannot ensure population inversion, so their impact on resonant HHG originates from increased ionization probability. Multiphoton ionization can indeed take place even when tunneling ionization is a dominant mechanism. Although the stability of multiphoton resonance in strong laser field is questionable due to AC Stark shift, any growth of ionization increases HHG efficiency provided the phase matching conditions are not modified greatly, so multiphoton resonances during ionization should not be discarded from consideration. Meanwhile, the assumption of ionization assisted by multiphoton resonances as the only source of resonant HHG enhancement, especially when combined with single active electron (SAE) approximation, always predicts enhancement of a group of harmonics, which has not been achieved in typical resonant HHG experiments (see for example [4]).

A semi-classical 4-step model has been suggested in [17], which was able to describe most of the properties of resonant HHG in SAE approximation. The additional fourth step in this model is described by cross-section of electron transition to autoionizing (AI) state. This model gives reasonably good qualitative estimates of the efficiencies of resonant HHG for different experimental conditions by substituting experimentally measured decay widths of the resonant levels into SAE-based analytical formula to account for many-electron effects. There are however some uncertainties within this model, because SAE approximation does not consider real structure and dynamics of intra-atomic electronic structure. Namely, the electrons responsible for the resonant transitions with high oscillator strength definitely belong to inner shells of the systems in which resonant HHG was experimentally demonstrated. These electrons are in general very unlikely to be ionized directly by tunneling. So the corresponding excited states are not necessarily the AI states of the atomic systems, even if the energy of resonant transition is close to the ionization energies of the atoms. One should also take into consideration the dressing of higher Rydberg states, which may greatly modify the real AI states of the system.

Another common drawback of all models of resonant HHG, which assume the population of certain resonant level, is the unclear physical nature of transition of electron to the ground state with corresponding emission of coherent radiation at the harmonic frequency. If we consider these transitions as spontaneous due to finite lifetime of the resonant level or another laser-dressed state then the coherence and duration of the resonant radiation will differ greatly compared to non-resonant harmonics. If the process is considered a stimulated emission then the absence of population inversion will lead to decrease of harmonics near the resonance due to higher probabilities of stimulated absorption even when the degeneracy of the resonantly populated state is high. Experimental confirmation of the existence of spontaneous part of

resonant harmonics is an important tool for verification of the proposed approaches. It is still more favorable to consider depletion of resonantly populated level as a lasing without inversion (LWI) process, which cancels the stimulated absorption cross-section due to interference of two absorption channels in the presence of two fields coupled to the corresponding transitions [18].

In this section, we analyze recently introduced model of resonant high-order harmonic generation in multi-electron systems [19]. We follow the theory of resonant elastic scattering in the presence of energetically forbidden inelastic scattering channel in the approximation of strong coupling of two scattering channels. It will be shown that inelastic scattering channel cannot be completely closed and is extremely important for LWI processes within resonant HHG. The nature of this approach is similar to the model of channel closing, which has been successfully applied to studies of anomalous above-threshold ionization (ATI) spectra near ponderomotively upshifted Rydberg states [20, 21]. The experimental demonstration of the enhancement of different harmonic orders in the In plasma using the 806, 1431, and 1521 nm pumps is also discussed and compared with theoretical model.

## 1.2. Theory

Quantum mechanical simulation was performed to ensure that the excited state can in fact be populated in HHG experiments by inelastic scattering. The main part of any HHG simulation is the solution of time-dependent Schrödinger equation (TDSE). Complexity of wavefunction for systems with more than two degrees of freedom was the reason to restrict most of HHG simulations to SAE problems. Nowadays there are only two ways to make a TDSE solution feasible for multi-electron systems, which are based on time-dependent density functional theory (TDDFT) and multiconfigurational time-dependent Hartree-Fock (MCTDHF) approach, respectively. Although TDDFT calculations are much faster for large problems, they are not very convenient in investigation of the nature of HHG, because nothing can be said about which electrons actually participate in the process. Additionally, available TDDFT solution packages (Octopus [22], GPAW [23]) are restricted to plane-wave basis functions, which is reliable for most solid-state physics problems, but not guaranteed to give proper picture of ionization. In the discussed approach, the MCTDHF will be used, which not only gives a good combination of exactness of direct TDSE solution and speed of Hartree-Fock (HF) approximation, but also has a support of system's splitting, not included in HF approach.

The MCTDHF approach treats the wavefunction of multi-electronic system as

$$\Psi(Q_1, \dots, Q_f, t) = \sum_{j_1=1}^{n_1} \dots \sum_{j_f=1}^{n_f} A_{j_1 \dots j_f}(t) \prod_{\kappa=1}^f \phi_{j_\kappa}^{(\kappa)}(Q_\kappa, t), \quad (1)$$

where  $Q_1, \dots, Q_f$  are the coordinates of electrons,  $A_{j_1 \dots j_f}$ —antisymmetrized A-vector for all  $n_\kappa$  time-dependent expansion functions  $\phi_{j_\kappa}^{(\kappa)}$  for every degree of freedom  $\kappa$ . Setting  $n_\kappa = n_1$  describes direct solution of TDSE and  $n_\kappa = 1$  simplifies the wavefunction to ordinary time-dependent Hartree–Fock approximation.

The equations of motion in the MCTDHF approach are derived from modified variational principle

$$\left\langle \delta \Psi_{\text{MCHF}}(t) \left| i \frac{d}{dt} - H(t) \right| \Psi_{\text{MCHF}}(t) \right\rangle = 0 \forall t. \quad (2)$$

For the solution of MCTDHF equations of motion the Heidelberg MCTDH package [24–26] was used, which has a good support of various basis functions in discrete variable representation (DVR).

The pseudopotentials for indium ionic backgrounds have been generated by means of OPIUM pseudopotential generator [27] for neutral, singly and doubly ionized indium. Resonant HHG in indium is attributed to  $4d^{10}5s^2 \ ^1S^0 \rightarrow 4d^9 5s^2 5p \ ^1P_1$  transition in  $\text{In}^+$  ion [2], so only three-electron system is sufficient for this simple case, if correct pseudopotentials are chosen. However, when there are multiple excitations, the potential changes non-adiabatically, so for example, in case of two-particle impact excitation the Hamiltonian will have the form:

$$\hat{H} = \begin{pmatrix} H_{11} & H_{12} \\ H_{21} & H_{22} \end{pmatrix}, \quad (3)$$

where  $H_{11}$  is the neutral potential,  $H_{21}$  and  $H_{12}$  are the corresponding potentials for the 1st and the 2nd core electrons being removed, and  $H_{22}$  is the potential for both core electrons being excited. The states are electronically coupled to each other. The resulting HHG spectrum was obtained by Fourier transformation of the induced dipole.

As a driving pulse the Gaussian-shaped linearly polarized beam with FWHM of 35 fs and carrier frequency of 0.057 a.u. ( $\lambda = 800$  nm), peak intensity  $5 \times 10^{14} \text{ W cm}^{-2}$  and Gaussian-shaped envelope was used for calculations. Utilization of angular degrees of freedom for linearly polarized pump may seem questionable, but for given pseudopotentials there is a support of scattering as well. This assumption means that change of orbital momentum of every particle may modify its energy in such way, that scattering will in fact be more probable than direct fall on its place, which is achieved by electronic coupling of potential

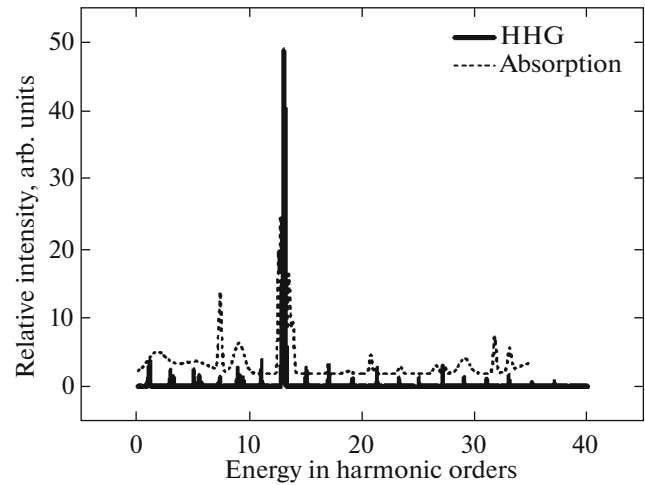


**Fig. 1.** Absorption spectrum of singly charged indium ion (dashed line, shifted by 2 units of relative intensity for better visibility) and resonant HHG spectrum (solid line) of the full system. Reproduced from [19] with permission from IOP Publishing.

energy surfaces with fixed orbital momentum to each other.

In Fig. 1 (dashed line), the absorption spectrum of a given system (indium ion, external electron removed, that is,  $H_{11}$  pseudopotential) is presented, which has been obtained by adding impulse to every electron in it and letting the system propagate freely for a long time (35 fs) and taking spontaneous emission spectrum afterwards. It is seen that there are some prominent absorption peaks in the area of 13th harmonic of 800 nm radiation, which can be predicted even from time-independent simulations. Then propagation of the system in a laser field was performed, which allowed to estimate HHG (Fig. 1, solid line). The cutoff was observed for the 39th harmonic and nonresonant harmonics had approximately same intensity in the plateau region. It is actually not surprising that resonant HHG has been observed, although with the intensity only 10–20 times higher than non-resonant harmonics, which is less than this harmonic enhancement obtained from experimental studies [2–4].

The population of excited state had time-dependent peaks (Fig. 2) with maximums close to instants when kinetic energy at return time is in general very close to that of resonant 13th harmonic. On the contrary, if resonant HHG would originate from the accelerated particle itself (direct recombination or electron capture), these peaks for indistinguishable particles would correspond to instants when kinetic energy at instant of recombination is equal to the energy of resonant harmonic minus ionization energy and for distinguishable particles there should have been no clear dependence at all. It is seen that only the kinetic energy of the accelerated particle is transferred

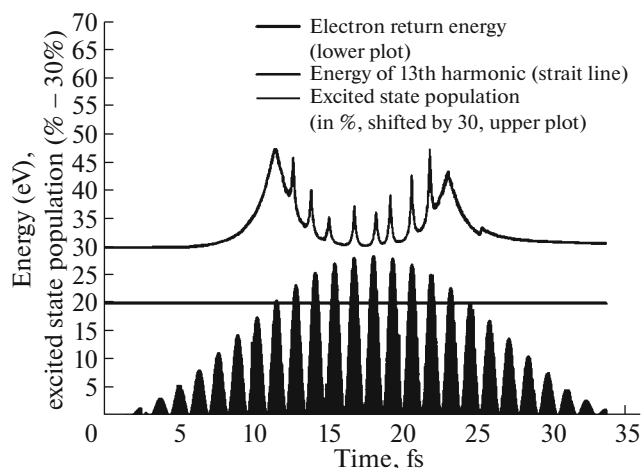


**Fig. 2.** Time dependence of the electron return energy (black area) and the excited state population (blue line, online available) for 35 fs pulses with Gaussian envelope; peak intensity:  $5 \times 10^{14} \text{ W cm}^{-2}$ . The maximum excited state population reached 17.5% (upper blue line and shifted upwards by 30 units for better visibility). Reproduced from [19] with permission from IOP Publishing.

for the excitation of another one, so collision excitation of inner electrons during inelastic scattering is possibly the base of resonant HHG. The population of the excited state also experiences some Rabi-like oscillations which can in principle show the possibility LWI processes.

The population in Fig. 2 is normalized to 13 for better visibility, and 13 corresponds to the maximum observed occupation of excited state of approximately 17.5%, which means that there is no population inversion during HHG process, so stimulated-emission based enhancement is not possible. One can deduce then, that resonant HHG is also in general a spontaneous emission.

### 1.3. Experiment and Discussion

To compare the modeling of resonance enhancement with experiment the following studies were carried out, which demonstrated the enhancement of different harmonics in the vicinity of the  $4d^{10}5s^2 \ ^1S_0 \rightarrow 4d^9 5s^2 5p \ ^1P_1$  transition in In II ion (19.92 eV, 62.24 nm). The  $gf$  value, the product of the oscillator strength  $f$  of a transition and the statistical weight  $g$  of the lower level, of this transition has been calculated to be  $gf = 1.11$  [28], which is more than 12 times larger than that of any other transition from the ground state of In II. This transition is energetically close to the 13th harmonic ( $h\nu_{H13} = 19.99 \text{ eV}$  or  $\lambda = 62 \text{ nm}$ ) of 806 nm radiation, the 23rd harmonic ( $h\nu_{H23} = 19.93 \text{ eV}$  or  $\lambda = 62.21 \text{ nm}$ ) of 1431 nm radiation, and the 25th harmonic ( $h\nu_{H25} = 20.38 \text{ eV}$  or  $\lambda = 60.84 \text{ nm}$ ) of 1521 nm radiation, thereby allowing the resonance-

induced enhancement of their intensity provided the plasma conditions allow maximally efficient harmonic generation.

The details of experimental setup are described elsewhere [29, 30]. Briefly, the experimental setup consisted of a Ti:sapphire laser, a traveling-wave optical parametric amplifier (OPA) of the white-light continuum, and a HHG scheme using propagation of the amplified signal pulses from the OPA through the extended laser-produced plasma (LPP). Part of the amplified radiation with pulse energy of 6 mJ was separated from the whole beam and used as a heating pulse for homogeneous plasma formation using a 200 mm focal length cylindrical lens installed in front of the extended (5 mm) indium target placed in the vacuum chamber. We analyzed the indium plasma as the medium for harmonic generation using the tunable and fixed sources of ultrashort pulses. The remaining part of the amplified radiation (806 nm, 64 fs) was delayed with regard to the heating pulse and propagated through the LPP. Another pumps of plasma were the signal pulses from OPA. The signal pulses from the OPA allowed tuning along the 1200–1600 nm. As it was mentioned above, we used the 1431 and 1521 nm pumps (70 fs). These driving pulses were focused at a distance of  $\sim 150 \mu\text{m}$  above the target surface. The plasma and harmonic emissions were analyzed using an extreme ultraviolet (XUV) spectrometer.

The experiments were carried out using both the single-color (806 nm) and two-color (1431 nm + 715.5 nm, 1521 nm + 760.5 nm) pumps of the LPP. The reasons for using the double-beam configuration to pump the extended plasma is related to the small energy of the driving near infrared (NIR) signal pulses ( $< 1 \text{ mJ}$ ). The  $I_H \propto \lambda^{-5}$  rule ( $I_H$  is the harmonic intensity and  $\lambda$  is the driving field wavelength) led to a significant decrease of harmonic yield in the case of longer-wavelength sources compared with the 806 nm pump and did not allow the observation of strong harmonics from the single-color NIR (1431 nm or 1521 nm) pulses. Because of this we used the second-harmonic (H2) generation of the signal pulse to apply the two-color pump scheme (NIR + H2) for plasma HHG. A 0.5-mm-thick beta barium borate crystal was installed inside the vacuum chamber on the path of focused signal pulse. The conversion efficiency of 715.5 nm and 760.5 nm pulses was  $\sim 15\%$ . The two orthogonally polarized pump pulses were sufficiently overlapped both temporally and spatially in the extended plasma, which led to a significant enhancement of odd harmonics, as well as generation of even harmonics of similar intensity as the odd ones.

Upper panel of Fig. 3 shows the plasma emission spectrum of indium plasma at the conditions of ablation, which do not allow efficient HHG. The harmonics generated in the indium plasma at the conditions when plasma emission was suppressed due to lower

fluence of heating pulses. Three bottom panels correspond to the latter conditions. In the case of 806 nm pump (second panel from the top), extremely strong 13th harmonic (H13) dominated the whole spectrum of emission. This harmonic was close to the 62.24 nm transition of In II shown as the solid line. Harmonic H13 was 15 to 40 times stronger than the neighboring harmonics depending on the plasma formation conditions.

The use of the two-color pump of NIR pulses (1431 nm + 715.5 nm, third panel from the top) also demonstrated the enhancement of harmonics in the vicinity of 62.24 nm transition of indium ion. One can see the enhancement of odd and even harmonics close to this wavelength. Harmonic H23 exactly matched with the above resonance transition and correspondingly showed highest yield. In the case of another two-color pump (1521 nm + 760.5 nm, fourth panel from the top) the optimal conditions of most efficient conversion were maintained for the H25.

Thus the transition of In II significantly affected the harmonic spectrum generating from the indium LPP. Notice that application of most other targets did not lead to enhancement of specific harmonic but rather to the featureless homogeneous harmonic distribution gradually decreasing up to the cut-off region. These studies confirmed the earlier reported studies on the significant influence of some ionic transitions on the harmonic distribution, which were also observed in the case of Cr, Mn, Sn, and some other plasmas. The enhancement factors of specific harmonics noticeably depended on the oscillator strengths of the involved ionic transitions. Note that in some cases the conditions for resonant recombination were fulfilled for more than one harmonic provided two-color fields were used. So there should not be a single resonance populated during HHG. Any multiphoton-based resonant excitation cannot explain such multiple resonant enhancement, while our approach for resonant HHG excitation by inelastic scattering remains valid as inelastic scattering channels of different spectral terms (here  $4d^{10}5s^x5p^y \rightarrow 4d^95s^x5p^{y+1}$ ) can be populated by accelerated electron with probability proportional to square of oscillator strength. The radiation of harmonics is also the stimulated emission as resonant HHG greatly decreased at conditions of spectral detuning of NIR pulses from resonances. The lifetime of resonant state is also much greater than duration of both main pulse and resulting harmonics to consider a significant spontaneous emission at harmonic frequency an important process. It has been shown both theoretically and experimentally for In, Sn, Sb, Cr that electronic transitions from inner  $d$ -subshell to outer  $p$ -subshell (that corresponds to the subshell where the first detached electron originally resided) of species with different ionization degrees lie close to each other [31, 32]. Control of degree of ionization of laser plasma can thus be used to fine-tune the frequencies of harmonics, which can be resonantly

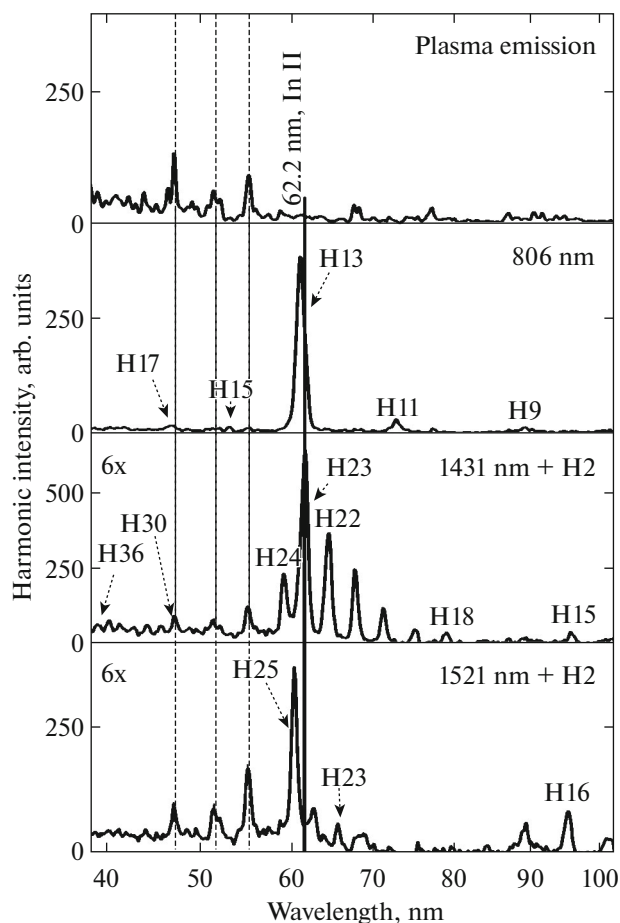


**Fig. 3.** Plasma and harmonic emission spectra generating in the indium plasma. Upper panel: plasma emission at over-excitation of ablating target. Second panel: single-color pump (806 nm) of optimally formed indium LPP. Third panel: two-color pump (1431 nm + 715.5 nm) of optimally formed indium LPP. Fourth panel: two-color pump (1521 nm + 760.5 nm) of optimally formed indium LPP. Two bottom panels were magnified with the factor of 6× compared with the second panel due to notably smaller conversion efficiency in the case of longer-wavelength pumps. Solid line corresponds to the In II transition responsible for the enhancement of harmonics. Dotted lines show the emission lines of In plasma observed in all these cases. Reproduced from [19] with permission from IOP Publishing.

generated. Model of multielectron resonant recombination restricts the choice of spectral transitions, which are promising to resonant HHG to permitted dipole transitions from the inner subshells to the lowest unoccupied subshell.

One should be very careful when speaking of precise coincidence of theoretical and experimental quantitative results. There is a problem of reproducibility of probe beam—experimental results are mostly averaged over shots, while in theory and calculations the laser beams tend to be perfect Gaussian beams. There is also a problem of phase matching which

relates to concentration of laser-ablated plasma particles. The concentration of laser plasma is in fact very difficult to be calculated. In addition, in most calculations the ablation beam itself is also not exactly reproducible. Every theory inflicts additional approximation errors. This all should be considered when respecting precision of calculation as the best proof for validity of theory. But the model potential in [17] has immense advantage of reducing a multi-electron problem to one-electron problem. So better binding of its parameters to spectral properties of given systems can be considered promising as well.

## 2. CONTROLLING SINGLE HARMONIC ENHANCEMENT IN LASER-PRODUCED PLASMAS

As was already mentioned, the resonance-induced enhancement of the harmonics of ultrashort pulses is one of the attractive features of coherent radiation frequency conversion in laser-produced plasmas, with the maximal enhancement factor of a single harmonic approaching 80 in the case of indium plasma. Notice that no experiments with gases showing the resonance enhancement of single harmonics have been reported so far. Why have resonant harmonics not been observed in gas media? The answer to this fundamental question is related to the basic principles of the role of ionic resonances in the enhancement of harmonics. Various factors prevented the observation of resonance enhancement. Among them are the self-absorption near the ionic transitions, which emit strong radiation in the extreme ultraviolet range, and the weak oscillator strength of these transitions. Furthermore, it is obvious that the choice of gases, mostly limited to a few noble gases, is dramatically narrow compared with that of solids, which includes almost all the periodic table predominantly containing the solid elements. Consequently, the probability of finding the appropriate resonance with high oscillator strength, which matches with some harmonics, is significantly smaller in the case of HHG in gases compared with HHG in plasmas. These conditions are rarely fulfilled, and if fulfilled they most probably occur in media produced during the ablation of thousands of solids rather than in a few gases. That is why the analysis of this phenomenon in plasma media has more chances of success.

In this section, we discuss the studies of a few plasma samples, which showed numerous cases of the coincidence of harmonics with some emission lines of corresponding ions. We analyze ionic transitions demonstrating high oscillator strengths, which are responsible for enhanced emission of a single order or group of harmonics. Meanwhile, plasma emission plays rather destructive role during HHG in the plasma plumes [33].

### 2.1. Featureless and Resonance-Enhanced Harmonic Distributions

In this subsection, we analyze the raw images of plasma and harmonic spectra from different LPPs. The reason in presentation of experimental data as the images appearing on the screen of computer rather than the groups of intensity distributions is caused by better viewing of obtained data and clear definition of the difference between the so called featureless group of harmonics and the group of harmonics containing a single enhanced harmonic. We would like to stress that the goal of discussed studies [33] was the qualitative definition of the influence of plasma emission on the harmonic conversion efficiency in different LPPs rather than the quantitative measurements of the gain of single harmonic in the plasmas where this process could be realized. Also notice that visual analysis of raw images of harmonic and plasma emission allows distinguishing these sources of radiation by their divergences. The vertical dimensions of the raw images of plasma emission, which characterize its divergence, were a few times larger compared with those of harmonics.

The saturated images were intentionally chosen to present the spectra for better viewing. Note that for the line-outs of the HHG spectra the unsaturated images were used. The X-axes are shown in the figure on the basis of the calibration of XUV spectrometer for better viewing of the distribution of harmonics along the short-wavelength region. The HHG spectrometer was calibrated using the plasma emission from the used ablated species, as well as other ablating targets.

Experimental setup was similar to the one described in Sec. 1. 5-mm-long Sb, Sn, Mn, Zn, Se, Cr, Ag, Au, Mg, Cd, and graphite samples were used as the targets for ablation and formation of extended homogeneous plasma. First set of studies was carried out in the plasmas where no resonance enhancement was observed. Figure 4a shows the plasma and harmonic spectra obtained during ablation of silver and gold targets. The plasma emission spectra were observed at the conditions of ablation at which the HHG could be realized at unfavorable conditions. These plasma spectra, as well as all other emission spectra obtained during ablation of targets, were registered at the conditions when femtosecond pulses did not propagate through the LPPs. Meanwhile, the HHG was performed at the conditions of optimal LPP formation. The term "optimal LPP formation" refers to maximal harmonic yield during propagation of femtosecond pulses through such plasmas. Both Ag and Au plasmas are the attractive media for extended harmonic distribution. The harmonics up to H63 and H57 (not shown in Fig. 4a) were generated in the silver and gold plasmas during propagation of 810 nm, 64 fs pulses through these LPPs. These distributions did not reveal any enhancement of some specific harmonic order but rather represent the plateau like shapes when

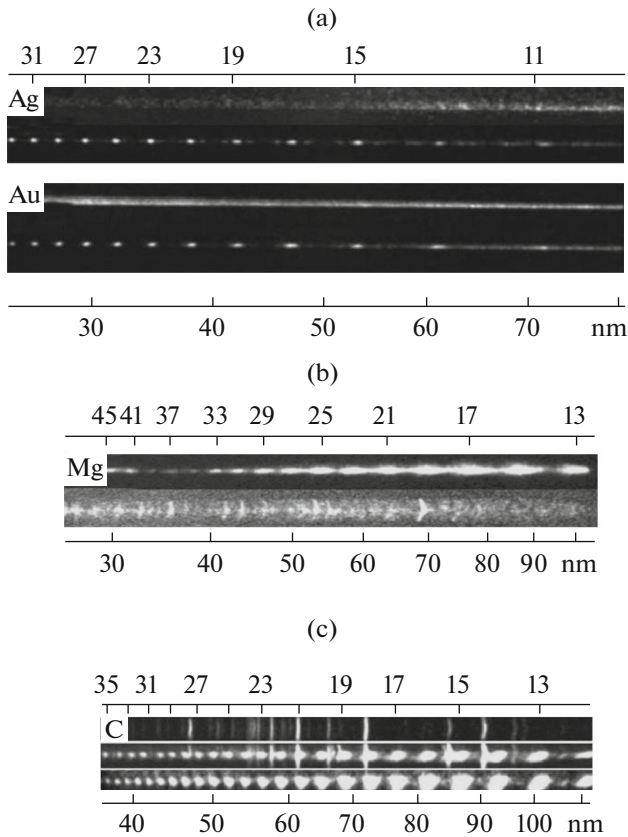


**Fig. 4.** Plasma and nonresonant harmonic spectra. (a) Raw images of plasma (upper panels) and harmonic (bottom panels) spectra obtained during ablation of Ag and Au targets and 810 nm femtosecond pulses propagation. Harmonic orders and wavelengths in this and most of other figures are shown on the upper and bottom axes respectively. (b) Raw images of harmonic (upper panel) and plasma (bottom panel) spectra obtained during ablation of Mg target and 1340 nm femtosecond pulses propagation. (c) Raw images of plasma (upper panel), plasma + harmonic (middle panel), and harmonic (bottom panel) spectra obtained during ablation of graphite target and 1340 nm + 670 nm femtosecond pulses propagation. Reproduced from [33] with permission from AIP Publishing.

the intensities of harmonics were approximately same along the whole spectral range of generation with some gradual decrease up to the cutoff orders. One can see that though H11 and H13 coincided with some emission lines of Ag and Au ions no enhancement of these harmonics was observed.

Similar pattern was obtained in the case of Mg (Fig. 4b) and graphite (Fig. 4c) plasmas. One can see that at least H19, H27, and H37 of the single-color pump (1340 nm, 70 fs) propagating through the magnesium plasma coincided with the plasma emission lines. However, neither enhancement nor decrease of these harmonics was observed in the case of HHG in this plasma, but rather gradual decrease of each next order of harmonics compared with previous one.

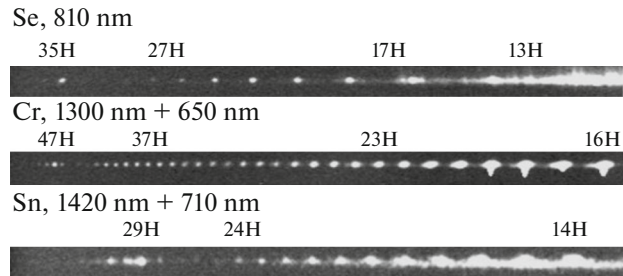


**Fig. 5.** Samples of resonance-induced enhancement of single harmonics in various plasmas. Upper, middle, and bottom panels correspond to the harmonic spectra generated in selenium, chromium, and tin plasmas using 810 nm, 1300 nm + 650 nm, and 1420 nm + 710 nm pumps respectively. One can see the enhanced H35 in the case of selenium plasma and 806 nm pump. In the case of chromium plasma, harmonics surrounded H47 were notably stronger compared with those in the range of H41–H45 in the case of 1300 nm + 650 nm pump. Similarly, tin plasma allowed observation of the enhanced harmonics in the vicinity of H29 of 1420 nm + 710 nm pump. Reproduced from [33] with permission from AIP Publishing.

The plasma emission from ablated graphite contained strong emission lines of carbon (upper panel of Fig. 4c). The propagation of the two-color pump (TCP, 1340 nm + 670 nm) through such plasma allowed generation of approximately equal odd and even harmonics of 1340 nm radiation up to the H43 (second panel). One can see that coincidence of a few harmonics with these emission lines did not cause the change of their intensity relative to neighbor orders. Moreover, as was mentioned above, a decrease of heating pulse energy on the target surface allowed formation of optimal graphite plasma resulting in noticeable enhancement of all harmonics (bottom panel; compare with middle panel). Again as in previous cases (Figs. 4a, 4b), the featureless harmonic spectrum, without the enhancement of a single harmonic, was obtained.

Most of plasmas producing on the targets representing the solid elements of periodic table allowed generation of harmonic spectra similar to those shown in Fig. 4. Meanwhile, a few solid elements showed outstanding features being used for LPP formation and HHG. In Fig. 5, three samples of harmonic spectra demonstrating the enhanced single harmonic, or group of harmonics, in different ranges of XUV using the selenium, chromium, and tin LPPs, are shown.

The single-color pump (SCP) of Se plasma using 810 nm radiation allowed odd harmonics generation up to H27 using the optimally formed LPP. The growth of heating pulse fluence on the surface of ablating target led to appearance of plasma emission in the range of H10–H15 and the decrease of a whole yield of harmonics (Fig. 5, upper panel). Meanwhile, this over-excitation of target caused the growth of population of some ionic states, which allowed the obser-

vation of an enhanced single harmonic (H35) far from the whole set of harmonics. This harmonic was visibly stronger than the lower-order ones (H23–H33), contrary to commonly observable patterns of lower intensities for the higher orders compared with lower-order ones. In fact, the neighboring harmonics around H35 were barely seen in this spectrum.

The HHG spectrum from Cr plasma also showed the gradual decrease of harmonic yield up to H42 using TCP (1300 nm + 650 nm). At higher excitation of target, we observed a group of harmonics centered around H47, apart from the set of lower-order harmonics (second panel).

The third sample of unusual distribution of harmonic spectra was observed during experiments with tin plasma (third panel). The TCP (1420 nm + 710 nm) of over-excited plasma caused appearance of both the mixture of harmonic and plasma emission in the longer wavelength range of XUV and the group of enhanced harmonics (H31, H30, and especially H29). Notice the absence of H25–H27 in this spectrum.

Those results were compared with the spectroscopic analysis of the properties of specific ionic transitions of Se, Cr, and Sn. The resonance-enhanced single harmonic observed in selenium plasma had a shortest wavelength (H35 of 802 nm pump,  $\lambda = 22.9$  nm,  $E = 54.1$  eV) reported so far among other resonance enhanced processes [34]. The doubly ionized selenium atom has the ground configuration  $4s^24p^2$  and the excited configurations  $4s^4p^3$ ,  $4s^24pnd$  ( $n > 4$ ), and  $4s^24pns$  ( $n > 5$ ). The photon energy studied in previous spectroscopic experiments with Se plasma was ranged between 18.0 and 31.0 eV [35, 36]. However, they also reported the strong third-order line corresponded to the 54.62 eV energy ( $\lambda = 22.7$  nm), without the deliberation of the origin of this transition. Note that this transition is close to the enhanced H35 in our experiments. Probably, this transition can influence the nonlinear optical response of selenium plasma in this spectral region.

Previous studies of photoabsorption and photoionization spectra of Cr plasma in the range of 41–42 eV have demonstrated the presence of strong transitions, which could be responsible for such a pattern of harmonic spectrum. In particular, the region of the “giant”  $3p \rightarrow 3d$  resonance of Cr II spectrum was analyzed in [37]. The role of the  $3d^5(^6S)$  state in determining the special position of Cr among the  $3d$  elements was emphasized and the strong transitions, which could both enhance and diminish the optical and nonlinear optical response of the plume, were revealed. Some previous studies of chromium plasma revealed the enhancement of single harmonics in the case of different sources of driving pulses. Particularly, H29 ( $\lambda = 27.6$  nm) of 800 nm pump was noticeably stronger than other harmonics [38].

In past work, the strong Sn II ion has been shown to possess a strong transition  $4d^{10}5s^25p^2P_{3/2}-$

$4d^95s^25p^2(^1D)^2D_{5/2}$  at the wavelength of 47.20 nm [39]. The  $gf$  value of this transition has been calculated to be 1.52, and this value is five times larger than other transitions from the ground state of Sn II. Therefore the enhancement of the H29 ( $\lambda = 48.9$  nm) using the 1420 nm + 710 nm wavelength pump can be explained as being due to optimal closeness to the above transition. The resonance enhancement of single harmonic (H17 of 795 nm laser,  $\lambda = 46.8$  nm) has previously been observed and attributed to the influence of the same transition [40].

These three samples of harmonic spectra point out the role of ablation conditions in the formation of the LPP allowing such an unusual distribution of harmonics appearing in the shorter wavelength range of XUV. During last decade this phenomenon was observed in the case of some ionic transitions the  $gf$  of which were significantly larger compared with similar parameters of other neighboring transitions in different spectral ranges [41–44]. Meanwhile, the role of plasma emission lines was yet examined. Below we show the comparative studies of plasma and harmonic spectra at the conditions of coincidence or mismatch of plasma and harmonic wavelengths.

## 2.2. Comparison of Plasma and Harmonic Spectra in the LPPs Allowing Generation of Resonantly Enhanced Harmonics

To analyze the role of the ionic transitions responsible for plasma emission on the enhancement of single harmonic one has to use a tunable source of femtosecond pulses. The pump wavelength was tuned using OPA, which allowed the variation of harmonic wavelengths in the vicinity of strong emission lines in the XUV range using Zn, Sb, Cd, and In LPPs. The fixed wavelength of pump radiation was also used to analyze the plasma and harmonic emission from Mn ablation. The data on the plasma emission of various elements were taken from the NIST Atomic Spectra Database [45].

**Zinc plasma.** Upper panel of Fig. 6a shows the raw image of zinc plasma emission where a few strong emission lines in the range of 65–90 nm dominated the XUV spectra. This spectrum was obtained at the unfavorable conditions for harmonic generation (i.e., at  $\sim 2$  J cm<sup>-2</sup> fluence of heating pulse), similarly to the LPP spectra shown in Fig. 4. At optimal conditions of zinc ablation when maximally efficient HHG was achieved a few plasma emission lines were still seen among the harmonics. Particularly, strong 67.8 nm emission line of Zn III attributed to  $3d^{10}-3d^94p$  transition appeared between H19 and H20 of 1320 nm + 660 nm pump (second panel). The same can be said about 75.5 nm emission line. The harmonic spectrum was extended up to H36. The H15 and H17, which coincided with 88.1 and 76.7 nm emission lines, appeared to be stronger than other neighboring har-

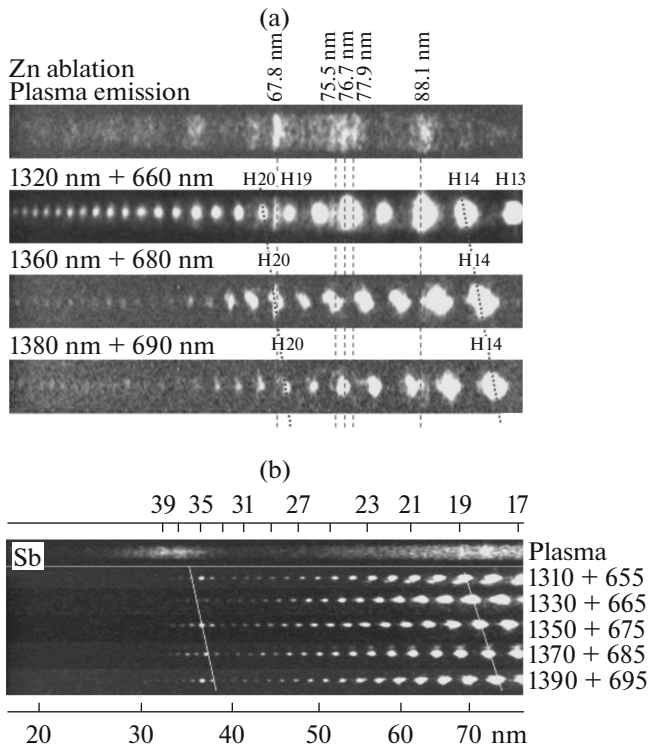


**Fig. 6.** (a) Raw images of plasma (upper panel) and harmonic (three other panels) spectra obtained during ablation of zinc. Harmonic spectra were tuned by changing the wavelength of driving NIR radiation and its second harmonic from 1320 nm + 660 nm (second panel from the top) to 1360 nm + 680 nm (third panel) and 1380 nm + 690 nm (fourth panel). Dashed lines show the positions of strong plasma emission lines in all four spectra. Dotted lines show the tuning of H14 and H20 at different pumps of plasma. The intensity of H20 remained approximately same during tuning through the strong resonance transition ( $\lambda = 67.8$  nm), while H17 was stronger in the case of 1320 nm + 660 nm pump. (b) Raw images of plasma (upper panel) and harmonic (five other panels) spectra obtained during ablation of antimony. Harmonic spectra were tuned by changing the wavelength of driving NIR radiation and its second harmonic from 1310 nm + 665 nm (second panel from the top) to 1390 nm + 695 nm (sixth panel) with a step of 20 nm. Solid lines show the tuning of H36 and H19 at different pumps of plasma. The harmonic orders shown on the top of images correspond to those generated using the 1310 nm + 655 nm pump. Most of harmonics remain same during variation of pump wavelength, excluding those in the region of 37.5 nm. Reproduced from [33] with permission from AIP Publishing.

monics. It was difficult to define whether this difference in harmonic intensities can be attributed to the influence of emission line or to the naturally stronger odd harmonics compared to the even ones.

To define the role of plasma emission lines the fluence of heating pulse was decreased and the harmonics were tuned (third panel, 1360 nm + 680 nm pump). In that case only 67.8 nm line remained in the spectrum while other plasma emission lines almost disap-

peared. The odd and even harmonics (at least up to H22) showed a gradual decrease of intensity for each next harmonic order, without any features indicating the resonance enhancement. The whole decrease of conversion efficiency compared with 1320 nm + 660 nm pump was caused by the higher energy of latter TCP compared with previous pump. This decrease of HHG conversion efficiency is further seen in the case of 1380 nm + 690 nm pump (fourth panel), which also confirmed our assumption about the negligible role of the ionic transitions responsible for plasma emission on the HHG.

The H17 of 1320 nm + 660 nm pump could be partially enhanced due to different processes. The involvement of 76.7 nm transition of Zn II on the variations of harmonic yield near this transition was earlier examined in [46] by using the model potential introduced in [17]. The width of resonantly enhanced H17 in those studies was close to that of other harmonics, both in calculated and experimental results, similarly to present data. Another case was observed in the case of 67.8 nm line. The enhancement region is narrower than the harmonic line width (third panel), so the shape of H20 is close to the one of surrounding harmonics but with a narrow maximum due to the possible resonant enhancement. Similar observation was reported using 775 nm, 4 fs probe pulses. The observations of the strong emission of 18.3 eV transition ( $\lambda = 67.8$  nm,  $3d^{10}-3d^94p$ ) of Zn III at the conditions of plasma excitation by a few cycles of broadband pulses centered at 775 nm was attributed to the enhancement of part of the 11th harmonic of this radiation, although the wavelength of this harmonic (70 nm) did not exactly match the wavelength of  $3d^{10}-3d^94p$  transition, which has an oscillator strength significantly greater than other lines in this spectral region [47]. In those studies, the narrowband-enhanced emission was similar to that observed here and could also be attributed to the influence of resonance and propagation processes.

**Antimony plasma.** Another example demonstrating the enhancement of single harmonic by tuning through the ionic transition possessing high  $gf$  rather than strong plasma emissions was demonstrated in the case of antimony plasma. This plasma has two strong ionic transitions in the region of generating harmonics. The XUV spectra of antimony plasma have been analyzed in [48]. The oscillator strengths of  $4d^{10}5s^22p^3P_2-4d^95s^25p^3^3D_3$  and  $4d^{10}5s^22p^1D_2-4d^95s^25p^3^3F_3$  transitions have been calculated to be 1.36 and 1.63, respectively, which were a few times larger than those of the neighboring transitions. These strong Sb II transitions ( $4d^{10}5s^22p^3P_2-4d^95s^25p^3^3D_3$  and  $4d^{10}5s^22p^1D_2-4d^95s^25p^3^3F_3$ ) at the wavelengths of 37.82 nm and 37.55 nm could be responsible for the enhancement of harmonics in the vicinity of these transitions.

Upper panel of Fig. 6b shows two groups of plasma emission comprising the continuum and emission lines. Notice that there are no peculiar emission lines in the vicinity of 37–38 nm. Strongest emission line seen only at 32.5 nm, quite far from the spectral range of expected enhancement of the nonlinear optical processes.

The application of TCP allowed a significant enhancement of harmonic yield compared with SCP. Two-color pump was gradually tuned between 1310 nm + 655 nm to 1390 nm + 695 nm with a step of MIR pulses of 20 nm (second to sixth panels). The lower-order harmonics remained approximately same during this procedure. The harmonic orders shown in upper axis are attributed to those in the second panel. The white solid line at the right side of this picture shows the tuning of H19. No significant changes in intensities of this harmonic seen while tuning between the two plasma emission lines shown in the upper panel. The second group of harmonics appears in the 36–38 nm region. The white solid line at the left side of picture shows the tuning of H36. One can see a significant change of the intensity of this harmonic, with maximal conversion efficiency at  $\sim 37.3$  nm. Probably, the shorter-wavelength side of two abovementioned resonances is responsible for better enhancement of the harmonics tuning in this region. The reasons for this peculiarity could be related with the propagation effect, when the phase matching conditions became better for the system possessing lower difference between the wave numbers of pump and harmonic emissions due to anomalous dispersion in this side of resonances. These lines are not seen in the plasma emission spectrum (see the left group of lines and continuum appearing in the 28–36 nm range on the first panel). The efficiency of each neighboring harmonics in this region depended to the closeness with the  $4d^{10}5s^22p^3\ ^3P_2-4d^95s^25p^3\ ^3D_3$  and  $4d^{10}5s^22p\ ^1D_2-4d^95s^25p^3\ ^3F_3$  transitions of Sb II ion.

**Cadmium plasma.** The relative intensities of the H15 generating in Cd plasma were tuned by changing the SCP from 1360 nm to 1320 nm, as shown in Fig. 7a (two bottom panels). One can clearly see the relatively equal intensities of other harmonics in the case of 1320 nm and 1360 nm pumps. Meanwhile, the tuning of pump and harmonic wavelengths towards the longer-wavelength region significantly changed the pattern of H15. Harmonic H15 ( $\lambda = 90.7$  nm) using 1360 nm pump became significantly stronger than the H15 obtained using 1320 nm radiation. The emission lines from Cd plasma (upper panel) were far from the region of H15. Thus the influence of the transitions responsible for plasma emission was insignificant from the point of view of variations of the relative intensities of this harmonic.

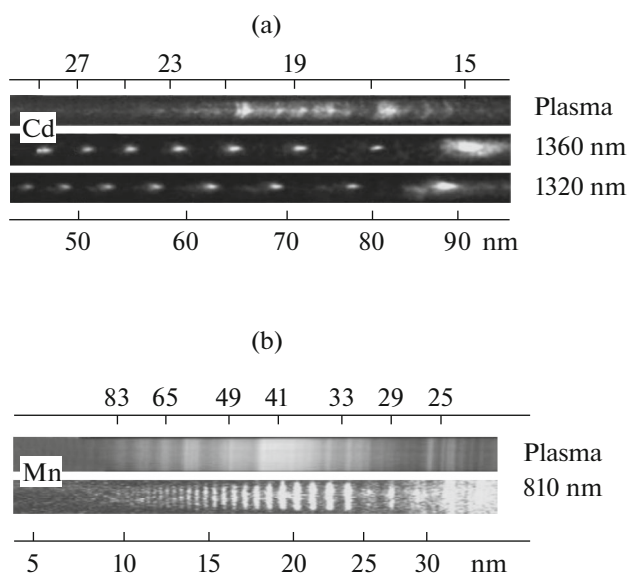


**Fig. 7.** (a) Raw images of plasma (upper panel) and harmonic (two bottom panels) spectra obtained during ablation of cadmium. Harmonic spectra were tuned by changing the wavelength of driving NIR radiation from 1320 nm (third panel from the top) to 1360 nm (second panel). The harmonic orders shown on the top of images correspond to those generated using the 1360 nm pump. (b) Raw images of plasma (upper panel) and harmonic (bottom panel) spectra obtained during ablation of manganese. The intensity of H33 of the 810 nm pump was notably stronger than lower-order harmonics. Adapted from [33] with permission from AIP Publishing.

**Manganese plasma.** The final example of harmonic enhancement is shown in Fig. 7b. The Mn plasma was emitted in a broad short-wavelength region (10 to 35 nm, upper panel) during over-excitation of target by 370 ps pulses (i.e., at a fluence of  $1.9\text{ J cm}^{-2}$ ). The harmonics at weaker ablation ( $1.2\text{ J cm}^{-2}$ ) were limited by H29. The growth of heating pulse fluence led to appearance of the extended group of harmonics starting from H33 and extended up to H83 (bottom panel). There was no relation between the emission lines and enhanced H33 and following harmonics. One can assume better conditions of enhancement for the H33 in the vicinity of the giant  $3p \rightarrow 3d$  resonances of Mn around the 51–52 eV range, where the metastable states of manganese are located [49]. Meanwhile there are no relations between the observed plasma emission lines (upper panel) and the harmonic enhancement in the region of  $\sim 24$  nm (bottom panel).

These studies have confirmed previous observations of resonance enhancement of harmonics in laser-produced plasmas [50–53] and paved the way for the nonlinear optical spectroscopy of plasma materials.

### 3. QUASI-PHASE-MATCHING OF HIGH-ORDER HARMONICS IN PLASMA: THEORY AND EXPERIMENT

#### 3.1. *Quasi-Phase-Matching in Gases and Plasmas*

Various methods have been implemented in the high-order harmonic generation in gases and plasmas to improve the conversion efficiency. In the case of harmonics generated in laser plasma they include the use of nanoparticles and clusters as harmonic sources, the use of various combinations of two- or three-color pumps, the application of extended plasma, the realization of the conditions of resonant amplification of single harmonic, and the formation of quasi-phase matching (QPM) between interacting waves. The latter of these techniques in combination with two-color pumping of plasma have demonstrated their attractiveness by increasing the conversion efficiency in various ranges of the extreme ultraviolet region [54]. Most of the previous studies of QPM were performed using conventional Ti:sapphire lasers and their second harmonics as the radiation sources. Meantime, the use of longer wavelengths of the laser sources can lead to a further increase of harmonic yield by applying the multi-jet plasmas compared with the extended homogeneous plasmas. Particularly, the tunable optical parametric amplifiers (OPA) generating in the near infrared region, and their second harmonics will allow to generate a wide range of wave sum and difference harmonics.

The phase mismatch between the interacting waves suppresses the HHG in the gas and plasma media. The dephasing between the propagating harmonic wave and laser-induced polarization is mainly caused by the dispersion of the medium and becomes essential in the presence of a significant number of free electrons. Due to the difference in the velocity of the waves, at some distance from the beginning of the medium, the phase shift becomes close to  $\pi$ . Beyond this distance, called the coherence length, the constructive accumulation of harmonic photons is reversed and the harmonic energy starts to decrease. Quasi-phase matching of interacting waves can significantly reduce the negative impact of phase mismatch as well as to increase the conversion efficiency in different parts of the XUV spectrum.

Quasi-phase matching has been demonstrated in gases [55–60] and multi-jet plasma formations [61, 62]. Though not new for the case of gas harmonics, this approach recently allowed a significant increase of harmonic yield in the case of modulated plasmas. Moreover, the so-called “self-probing” schemes to extract structural and dynamical information about the generating medium from the intensity measurements of HHG, which have already been reported in the case of gas targets, are extended to plasma targets. The implementation of this concept for the case of plasma harmonics widely broadens the field of study due to the overwhelming prevalence of the ablated

solid species used in the latter case over the few gas types routinely exploited in conventional HHG.

The key enabling technology for this research is the capability of laser ablation to put atoms and molecules from solids into gas phase at appropriate densities [61–63]. This method of plasma formation also allows the analysis of the relative role of micro- and macro-processes in the enhancement of harmonic yield [64]. Such a concept can be useful for the formation of a group of harmonics when the phase-locking of the harmonics leads to the production of an attosecond pulse train. The comparative analysis of different sources of pump radiation (e.g., fixed-wavelength ones, such as Ti:sapphire lasers and their second harmonics, or those with tunable wavelengths, such as OPA and their second harmonics) allows defining the best schemes for enhancement of HHG in different spectral regions of XUV.

In this section, the QPM experiments, which were carried out using different ablated solids, are discussed. The application of tunable mid-infrared pulses and fixed wavelength 800-nm-class laser for the QPM of harmonics is also compared [65].

#### 3.2. *Experimental Arrangements*

Two laser sources were used for these studies. In both cases, the uncompressed radiation of the Ti:sapphire laser was used as a heating pulse (central wavelength  $\lambda = 806$  nm, pulse duration 370 ps, pulse energy up to  $E_{hp} = 4$  mJ) for plasma formation using a 200 mm focal-length cylindrical lens, which focused the pulse inside the vacuum chamber containing an ablating target to create the extended laser-produced plasma above the target surface (Fig. 8a). The focusing of the heating pulse on the target surface produced the extended non-perforated plasma. The intensity of the heating pulses on a plain target surface was varied up to  $5 \times 10^9$  W cm<sup>-2</sup>.

In the first set of studies, the compressed driving pulse from the same laser with the energy of up to  $E_{dp} = 5$  mJ and 64 fs pulse duration was used, 45 ns from the beginning of ablation, for harmonic generation in the plasma plume. The driving pulse was focused using a 400 mm focal-length spherical lens onto the prepared plasma from perpendicular direction, at a distance of  $\sim 100$   $\mu$ m above the target surface. The confocal parameter of the focused driving beam was 18 mm. The intensity of the driving pulse in the focal area was varied up to  $9 \times 10^{14}$  W cm<sup>-2</sup>. The harmonic emission was analyzed by an XUV spectrometer. A detailed description of XUV spectrometer was given in [9].

In the second set of studies, we pumped the OPA (HE-TOPAS Prime, Light Conversion) by 10 mJ, 806 nm, 64 fs pulses. Signal and idler pulses from the OPA allowed tuning within the 1170–1620 nm and 1580–2650 nm ranges respectively. The experiments

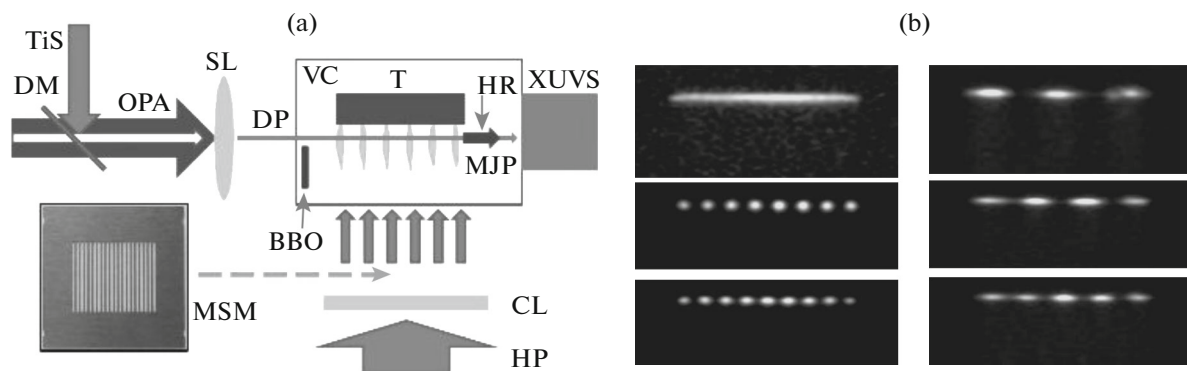


**Fig. 8.** (a) Experimental setup for the HHG in the multi-jet plasmas. HP, heating pulse; DP, driving pulse; CL, cylindrical lens; SL, spherical lens; MSM, multi-slit mask; DM, dichroic mirror; TiS, femtosecond radiation from Ti:sapphire laser; OPA, femtosecond radiation from optical parametric amplifier; VC, vacuum chamber; T, target; BBO, nonlinear crystal for second harmonic generation; HR, harmonic radiation; MJP, multi-jet plasma; XUVS, extreme ultraviolet spectrometer. (b) Shapes of silver plasma plumes produced at different modes of excitation of the target. Left picture shows the extended (5-mm-long) homogeneous plasma (upper panel), eight-jet plasma produced during installation of the MSM between cylindrical lens and target (middle panel), and nine-jet plasma produced during tilting the MSM at  $\theta = 25^\circ$  (bottom panel). Right picture shows the images of three-, four- and five-jet plasmas produced during placement of the MSM in different positions inside the telescope installed in front of the cylindrical lens. Reproduced from [65] with permission from Optical Society of America.

were carried out using  $\sim 1$ -mJ, 70-fs, 1310 nm signal pulses. The spectral bandwidth of these pulses was 50 nm. The intensity of the 1310 nm pulses focused by 400 mm focal length lens inside the extended plasma was  $\sim 2 \times 10^{14} \text{ W cm}^{-2}$ . Most of the experiments in this configuration were performed using two-color pump of the LPP.

Silver, indium and manganese were used as the targets for ablation. The reasons for choosing these samples are described in the following subsection. The size of the targets where the ablation occurred was 5 mm. To create multi-jet plasmas a multi-slit mask (MSM) was used. The slits of 0.3 mm width were spaced at 0.3 mm ( $d = 0.3 \text{ mm}$  and  $D = 0.6 \text{ mm}$ , see Fig. 8). The energy of the heating pulse decreased after propagation through the MSM. However the fluence of this radiation on the target surface remained unchanged, since the size of ablated area was also decreased. It means that the electron and plasma densities in the cases of extended homogeneous and multi-jet plasmas were almost equal.

### 3.3. Enhancement of Groups of Harmonics

In the case of homogeneous plasma target the silver plasma allows generation of almost ideal plateau-like distribution of harmonic intensities: the decrease of the latter starting from the 13th order (for 806 nm pump wavelength) is very slow up to the cut-off region ( $\sim \text{H61}$ ). Therefore the multi-jet target setup for silver plasma allows a clear observation of the quasi-phase-matching effect in different regions of XUV by variation of the plasma modulation parameter. This parameter actually represents the size of a single jet in the multi-jet plasma formed by installation of the MSM

between the focusing cylindrical lens and the target (inset in Fig. 8a).

Below some experimental results are shown, which can be compared with those obtained with the theoretical approach developed in previous section. Initially, we show the plasma shapes used for harmonic generation in the silver multi-jet plasmas produced at different modes of excitation of the target. Left picture in Fig. 8b shows the extended (5-mm-long) homogeneous plasma (upper panel), eight-jet plasma produced with MSM installed between the cylindrical lens and the target (middle panel), and nine-jet plasma produced as the MSM is tilted at  $\theta = 25^\circ$  (bottom panel). The picture in the right shows the images of three-, four- and five-jet plasmas produced as the MSM is placed in different positions inside the telescope installed in front of the cylindrical lens.

Figure 9a shows the harmonic spectra generated using the 806 nm pump in the extended (thin curve) and eight-jet (thick curve) silver plasmas produced by installation of the MSM ( $\theta = 0^\circ$ ). In the latter case we can see an enhancement of the group of harmonics centered at H33. The enhancement factor for the H33 was measured to be 11.

Stronger enhancement was observed in the case of two-color pump using the 1310 nm + 655 nm radiation (Fig. 9b). The two spectra shown in this figure represent the harmonic distributions captured under similar experimental conditions (energy of heating pulse, collection time of the harmonic spectra). Thin curve demonstrates the harmonic distribution obtained in the case of 5-mm-long silver plasma. The application of the MSM tilted at  $35^\circ$  drastically changed this distribution (thick curve). The group of harmonics centered in the vicinity of H37 was notably stronger com-

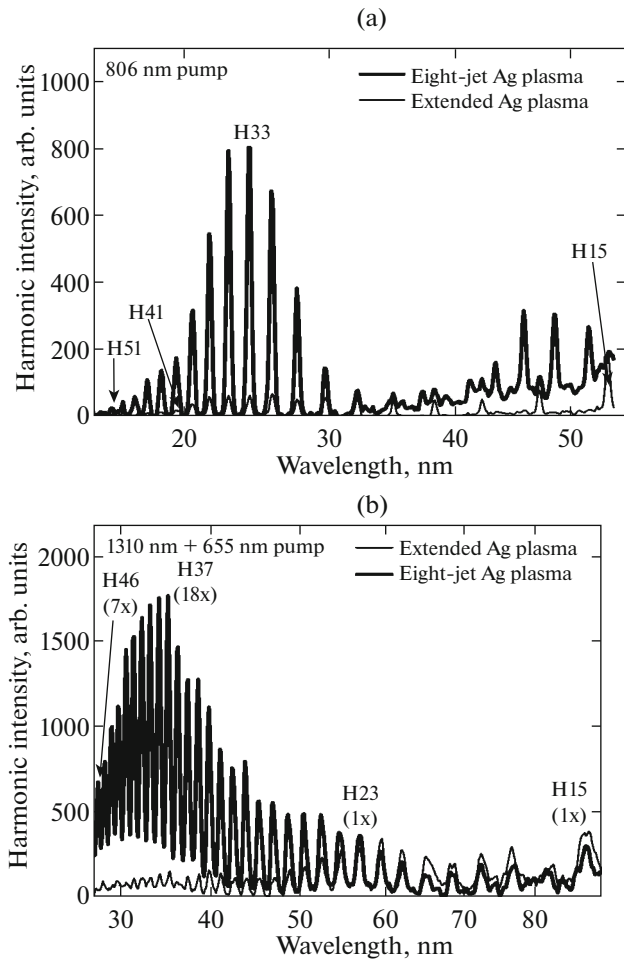


**Fig. 9.** (a) Harmonic spectra generated using the 806 nm pump in the extended silver plasma (thin curve) and eight-jet plasma produced by installation of the MSM containing 0.3 mm slits (thick curve). (b) Two-color pump using the 1310 nm + 655 nm radiation of the extended (thin curve) and eight-jet (thick curve) plasmas. The enhancement factors are shown below the harmonic orders. Reproduced from [65] with permission from Optical Society of America.

pared with previous case (the enhancement factor of the maximally enhanced H37 was  $\sim 18$ ), whereas the intensity of the lower-order harmonics decreased due to worsened conditions of the phase matching.

Indium plasma has an attractive feature allowing the observation of the joint influence of micro- and macro-processes on the harmonic efficiency. From the very beginning of plasma HHG studies, this plasma demonstrated the largest enhancement of a single (H13 of the 800-nm-class lasers) harmonic (see also Sec. 1). The reported enhancement factors were close to 80 [2, 66]. In our studies we used this plasma to demonstrate the QPM effect for the harmonics far from the spectral region (61 nm) where the resonance-induced harmonic occurred.

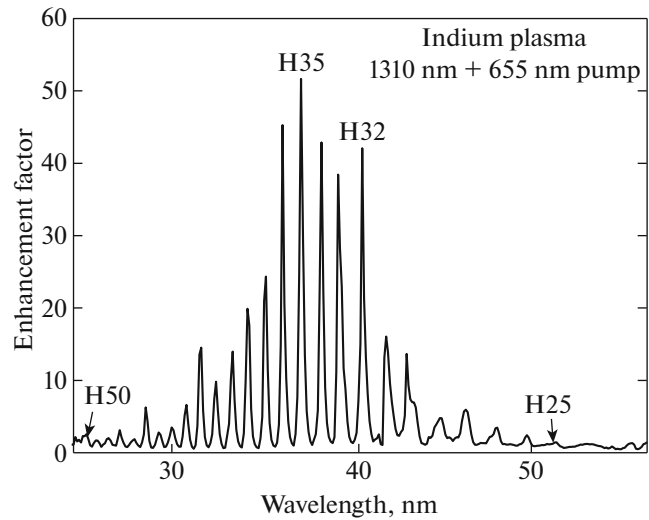


**Fig. 10.** The enhancement factor of the harmonics generated during two-color pump (1310 nm + 655 nm) of the modulated indium plasma containing eight jets. Reproduced from [65] with permission from Optical Society of America.

In the discussed studies, the variation of this spectrum was also analyzed while introducing the modulation of the extended (5 mm) indium plasma, similarly to the method described in the case of silver plasma. Particularly, a proper choice of the plasma conditions and pump wavelength can further optimize the QPM process using the described configuration. We were able to increase the enhancement factor of QPM harmonics by applying the wavelength of OPA allowing stronger emission (1310 nm), while exciting the indium target in such a manner that allowed us to maintain the QPM conditions for the group of lower-order harmonics (Fig. 10). The two-color pump (1310 nm + 655 nm) of this modulated plasma containing eight jets resulted in the enhancement factors of 40 to 50 for the group of harmonics centered at H35 ( $\lambda = 37.4$  nm). Some other features of the influence of micro- and macro-processes on the high-order harmonic generation in the laser-produced plasmas were recently analyzed in [64].

Finally, we discuss the observation of the QPM effect in the manganese plasma. The peculiarity of this material is the closeness of the QPM- and resonance-enhanced harmonics, which is in contrast to the case of indium plasma. The advantage of Mn plasma from the point of view of highest harmonic cut-off (i.e., above 100th orders) was reported in [67, 68], though the reasons of this peculiarity were not yet clearly explained. Note that the harmonic yield from this plasma was not as high as from some other plasma species. The use of a few-cycle pulses (3.5 fs) [69] has allowed the observation of a single (33rd) broadband harmonic.

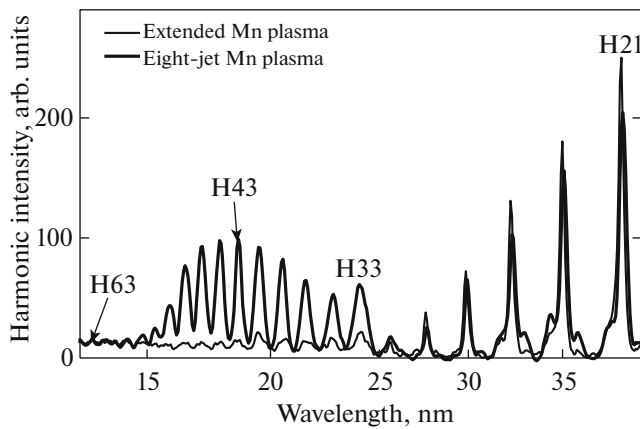


**Fig. 11.** Harmonic spectra generated during propagation of 806 nm pulses through the extended Mn plasma (thin curve) and eight-jet Mn plasma (thick curve). Reproduced from [65] with permission from Optical Society of America.

In the discussed studies, the Mn plasma produced by 370 ps pulses allowed generation of harmonics of 806 nm radiation with orders up to nineties. A weak excitation of target by 370 ps heating pulses ( $F_{hp} \approx 0.2 \text{ J cm}^{-2}$ ) led to plateau-like harmonic generation up to the cut-off (27th harmonic) similar to the one defined from the three-step model of HHG [10] for the singly charged Mn ions. Earlier, a growth of the harmonic intensity for the harmonics above H31 was attributed to the influence of the giant  $3p$ – $3d$  resonances of manganese ions [67]. Harmonics H27–H31 were significantly suppressed compared with the higher-order harmonics starting from H33.

The increase of the heating pulse fluence up to  $1.0 \text{ J cm}^{-2}$  caused a significant change of harmonic distribution in the case of imperforated 5-mm-long manganese plasma. Thin curve in Fig. 11 shows the generated spectrum, which points out the presence of only low-order harmonics (up to H29) in the case of imperforated Mn plasma, with some weak traces of higher orders. Replacement of the single extended nonlinear medium with the group of separated components of this medium (i.e., eight 0.3-mm-long plasma jets) drastically modified the generated harmonic spectrum (thick curve in Fig. 11). A group of strongly enhanced harmonics (H33–H51) prevailed in this spectral distribution. Notice that the resonance-enhanced harmonic (H33) was also enhanced, to some extent, due to QPM. The total enhancement factor of this harmonic was only  $\sim 4$  (more accurate measurement of this factor was problematic because of the low signal from the extended plasma target). Nevertheless, we can see that H33 is more intense than the neighbor harmonics (H31 and H35). The enhancement of the single harmonic is typical for resonance-induced enhancement. Thus the enhancement of H33 is due to both micro- and macro-processes.

#### 4. SUMMARY

Summarizing this review, the 4-step analytical model of resonant enhancement of HHG was extended to real systems with resonant transitions of inner-shell electrons. Resonant enhancement was explained by lasing without inversion in a three-level system of ground, excited and shifted resonant scattering states which are coupled to the fundamental field and its high harmonics. Role of inelastic scattering was studied by simulation of excited state's population dynamics. It was shown that maximal gain is achieved when the energy shift between the excited state and resonant scattering state is close to the energy of photon of fundamental field. The model of multielectron resonant recombination assumes excitation of inner electrons to resonant levels of the system by inelastic cross-section. Calculations show that resonant level is populated in HHG process by inelastic scattering. Combination of populated excited state and resonant elastic scattering state coupled to the main pump can lead to resonant HHG enhancement by LWI process. Resonant HHG can be considered as the experimental evidence of three-dimensional laser dressing of states. We have discussed the enhancement of harmonics in the In plasma using different pumps. Particularly, the 13th, 23rd, and 25th harmonics were notably enhanced compared with the neighboring harmonics using the 806, 1431, and 1521 nm pumps.

We analyzed the HHG in the Sn, Mn, Zn, Se, Sb, Cr, Ag, Au, Mg, C, and Cd plasmas, which showed numerous cases of the coincidence of harmonics with some emission lines of corresponding ions. However, this coincidence did not result in the enhancement of harmonics. We compared plasma conditions (spectral distribution of emission, excitation of high-charged ions, etc.) and harmonic generation. We also compared the cases of enhancement of single harmonic in the vicinity of some ionic transitions and featureless plateaulike HHG spectra from different plasma species to add more information about the role of plasma emission spectra. The comparative analysis of those two groups of plasma plumes have revealed the relative role of the strong emission lines and the transitions possessing high  $gf$  in the enhancement of single harmonics. This analysis of the harmonic spectra in the case of two abovementioned groups of LPPs have shown that ionic transitions demonstrating high oscillator strengths are responsible for enhanced emission of a single order or the group of harmonics. Finally, the experimental results of QPM for HHG in different plasmas using 806 nm and  $1310 \text{ nm} + 655 \text{ nm}$  were discussed. Quasi-phase-matching in the vicinity of the resonant harmonic in manganese has shown that harmonic yield can be enhanced through both these processes.

## REFERENCES

1. P. B. Corkum and F. Krausz, *Nat. Phys.* **3**, 381 (2007).
2. R. A. Ganeev, M. Suzuki, M. Baba, H. Kuroda, and T. Ozaki, *Opt. Lett.* **31**, 1699 (2006).
3. R. A. Ganeev, M. Suzuki, M. Baba, and H. Kuroda, *Appl. Phys. Lett.* **86**, 131116 (2005).
4. R. A. Ganeev, M. Suzuki, P. V. Redkin, M. Baba, and H. Kuroda, *Phys. Rev. A* **76**, 023832 (2007).
5. F. M. C. Faria, R. Copold, W. Becker, and J. M. Rost, *Phys. Rev. A* **65**, 023404 (2002).
6. R. Taieb, V. Veniard, J. Wassaf, and A. Maquet, *Phys. Rev. A* **68**, 033403 (2003).
7. T. Pfeifer, L. Gallmann, M. J. Abel, D. M. Neumark, and S. R. Leone, *Opt. Lett.* **31**, 975 (2006).
8. Z. Zeng, R. Li, Y. Cheng, W. Yu, and Z. Xu, *Phys. Scr.* **66**, 321 (2002).
9. A. V. Andreev, S. Y. Stremoukhov, and O. A. Shoutova, *J. Opt. Soc. Am. B* **30**, 1794 (2013).
10. P. B. Corkum, *Phys. Rev. Lett.* **71**, 1994 (1993).
11. L. Plaja and L. Roso, *J. Mod. Opt.* **40**, 793 (1993).
12. M. Gaarde and K. Schafer, *Phys. Rev. A* **64**, 013820 (2001).
13. M. Plummer and C. J. Noble, *J. Phys. B* **35**, L51 (2002).
14. K. Ishikawa, *Phys. Rev. Lett.* **91**, 043002 (2003).
15. P. A. Oleinikov, V. T. Platonenko, and G. Ferrante, *JETP Lett.* **60**, 246 (1994).
16. D. B. Milosevic, *J. Phys. B* **40**, 3367 (2007).
17. V. Strelkov, *Phys. Rev. Lett.* **104**, 123901 (2010).
18. G. S. Agarwal, *Phys. Rev. A* **44**, R28 (1991).
19. P. V. Redkin and R. A. Ganeev, *J. Phys. B* **50**, 185602 (2017).
20. R. Kopold, W. Becker, M. Kleber, and G. G. Paulus, *J. Phys. B* **35**, 217 (2002).
21. G. G. Paulus, F. Grasbon, and H. Walther, *Phys. Rev. A* **64**, 021401 (2001).
22. A. Castro, H. Appel, M. Oliveira, C. A. Rozzi, X. Andrade, F. Lorenzen, M. A. L. Marques, E. K. U. Gross, and A. Rubio, *Phys. Status Solidi B* **243**, 2465 (2006).
23. J. J. Mortensen, L. B. Hansen, and K. W. Jacobsen, *Phys. Rev. B* **71**, 035109 (2005).
24. H.-D. Meyer, U. Manthe, and L. S. Cederbaum, *Chem. Phys. Lett.* **165**, 73 (1990).
25. U. Manthe, H.-D. Meyer, and L. S. Cederbaum, *J. Chem. Phys.* **97**, 3199 (1992).
26. M. H. Beck, A. Jackle, G. A. Worth, and H.-D. Meyer, *Phys. Rep.* **324**, 1 (2000).
27. I. Grinberg, N. J. Ramer, and A. M. Rappe, *Phys. Rev. B* **62**, 2311 (2000).
28. G. Duffy and P. Dunne, *J. Phys. B* **34**, L173 (2001).
29. R. A. Ganeev, *Opt. Spectrosc.* **122**, 964 (2017).
30. R. A. Ganeev, *Opt. Spectrosc.* **123**, 117 (2017).
31. R. A. Ganeev, P. A. Naik, H. Singhal, U. Chakravarty, V. Arora, J. A. Chakera, R. A. Khan, M. Raghuramaiah, S. R. Kumbhare, R. P. Kushwaha, and P. D. Gupta, *Opt. Spectrosc.* **102**, 949 (2007).
32. R. A. Ganeev, L. B. Elouga Bom, and T. Ozaki, *Opt. Spectrosc.* **104**, 258 (2008).
33. R. A. Ganeev, *J. Appl. Phys.* **121**, 133108 (2017).
34. R. A. Ganeev, M. Suzuki, S. Yoneya, and H. Kuroda, *J. Appl. Phys.* **117**, 023114 (2015).
35. A. Tauheed and A. Hala, *Phys. Scr.* **85**, 025304 (2012).
36. D. A. Esteves, R. C. Bilodeau, N. C. Sterling, R. A. Phaneuf, A. L. D. Kilcoyne, E. C. Red, and A. Aguilar, *Phys. Rev. A* **84**, 013406 (2011).
37. J. B. West, J. E. Hansen, B. Kristensen, F. Folkmann, and H. Kjeldsen, *J. Phys. B* **36**, L327 (2003).
38. R. A. Ganeev, L. B. ElougaBom, J.-C. Kieffer, and T. Ozaki, *Phys. Rev. A* **75**, 063806 (2007).
39. G. Duffy, P. van Kampen, and P. Dunne, *J. Phys. B* **34**, 3171 (2001).
40. M. Suzuki, M. Baba, R. Ganeev, H. Kuroda, and T. Ozaki, *Opt. Lett.* **31**, 3306 (2006).
41. R. A. Ganeev, H. Singhal, P. A. Naik, V. Arora, U. Chakravarty, J. A. Chakera, R. A. Khan, I. A. Kurlagin, P. V. Redkin, M. Raghuramaiah, and P. D. Gupta, *Phys. Rev. A* **74**, 063824 (2006).
42. M. Suzuki, M. Baba, H. Kuroda, R. A. Ganeev, and T. Ozaki, *Opt. Express* **15**, 1161 (2007).
43. R. A. Ganeev, Z. Abdelrahman, F. Frank, T. Witting, W. A. Okell, D. Fabris, C. Hutchison, J. P. Marangos, and J. W. G. Tisch, *Appl. Phys. Lett.* **104**, 021122 (2014).
44. R. A. Ganeev, J. Zheng, M. Wostmann, H. Witte, P. V. Redkin, and H. Zacharias, *Eur. Phys. J. D* **68**, 325 (2014).
45. A. Kramida, Y. Ralchenko, J. Reader, and NIST ASD Team, *NIST Atomic Spectra Database, Version 5.1* (Natl. Inst. Standards Technol., Gaithersburg, MD, 2013).
46. R. A. Ganeev, M. Suzuki, S. Yoneya, V. V. Strelkov, and H. Kuroda, *J. Phys. B: At. Mol. Opt. Phys.* **49**, 055402 (2016).
47. K. A. Dick, *Can. J. Phys.* **46**, 1291 (1968).
48. R. D'Arcy, J. T. Costello, C. McGuinness, and G. O'Sullivan, *J. Phys. B* **32**, 4859 (1999).
49. H. Kjeldsen, F. Folkmann, B. Kristensen, J. B. West, and J. E. Hansen, *J. Phys. B* **37**, 1321 (2004).
50. R. A. Ganeev, *Opt. Spectrosc.* **114**, 614 (2013).
51. R. A. Ganeev, *Opt. Spectrosc.* **120**, 575 (2016).
52. R. A. Ganeev, *Opt. Spectrosc.* **120**, 766 (2016).
53. R. A. Ganeev, *Opt. Spectrosc.* **122**, 250 (2017).
54. R. A. Ganeev, M. Suzuki and H. Kuroda, *J. Phys. B* **47**, 105401 (2014).
55. A. Paul, R. A. Bartels, R. Tobey, H. Green, S. Weiman, I. P. Christov, M. M. Murnane, H. C. Kapteyn, and S. Backus, *Nature (London, U.K.)* **421** (6918), 51 (2003).
56. J. Seres, V. S. Yakovlev, E. Seres, C. H. Strelti, P. Wobrauschek, C. H. Spielmann, and F. Krausz, *Nat. Phys.* **3**, 878 (2007).
57. L. Zheng, X. Chen, S. Tang, and R. Li, *Opt. Express* **15**, 17985 (2007).

58. A. Pirri, C. Corsi, and M. Bellini, *Phys. Rev. A* **78**, 011801 (2008).
59. V. Tosa, V. S. Yakovlev and F. Krausz, *New J. Phys.* **10**, 025016 (2008).
60. T. Fok, L. Wegrzynski, M. Kozlova, J. Nejd, P. W. Wachulak, R. Jarocki, A. Bartnik and H. Fiedorowicz, *Photon. Lett. Pol.* **6**, 14 (2014).
61. R. A. Ganeev, M. Suzuki, and H. Kuroda, *Phys. Rev. A* **89**, 033821 (2014).
62. R. A. Ganeev, *Opt. Spectrosc.* **121**, 614 (2016).
63. R. A. Ganeev, V. Tosa, K. Kovacs, M. Suzuki, S. Yoneya, and H. Kuroda, *Phys. Rev. A* **91**, 043823 (2015).
64. R. A. Ganeev, *J. Appl. Phys.* **119**, 113104 (2016).
65. V. V. Strelkov and R. A. Ganeev, *Opt. Express* **25**, 21068 (2017).
66. R. A. Ganeev, H. Singhal, P. A. Naik, V. Arora, U. Chakravarty, J. A. Chakera, R. A. Khan, I. A. Kulagin, P. V. Redkin, M. Raghuramaiah, and P. D. Gupta, *Phys. Rev. A* **74**, 063824 (2006).
67. R. A. Ganeev, L. B. Elouga Bom, J.-C. Kieffer, and T. Ozaki, *Phys. Rev. A* **76**, 023831 (2007).
68. R. A. Ganeev, M. Baba, M. Suzuki, S. Yoneya, and H. Kuroda, *J. Appl. Phys.* **116**, 243102 (2014).
69. R. A. Ganeev, T. Witting, C. Hutchison, F. Frank, M. Tudorovskaya, M. Lein, W. A. Okell, A. Zaïr, J. P. Marangos, and J. W. G. Tisch, *Opt. Express* **20**, 25239 (2012).